Journal of Power Sources 251 (2014) 488–495

Contents lists available at ScienceDirect

Journal of Power Sources

journal homepage: www.elsevier.com/locate/jpowsour

Oxidation study of coated Crofer 22 APU steel in dry oxygen

Sebastian Molin*, Ming Chen, Peter Vang Hendriksen

Department of Energy Conversion and Storage, Technical University of Denmark, Frederiksborgvej 399, 4000 Roskilde, Denmark

HIGHLIGHTS

- Dual layer coated Crofer 22 APU was tested at 800 °C–850 °C–900 °C in dry oxygen for 1000 h.
- Long term corrosion test (5000 h) was performed at 850 °C.
- Coating is very efficient in reducing corrosion rates.
- Temperature dependence of the corrosion rate indicated that Cr outward diffusion is a limiting reaction.
- Developed coating assures long lifetime of Crofer 22 APU steel for application as interconnect.

ARTICLE INFO

Article history:
Received 12 March 2013
Received in revised form
20 August 2013
Accepted 23 September 2013
Available online 2 October 2013

Keywords:
High temperature corrosion
Protective coating
Solid oxide electrolysis
Interconnect

ABSTRACT

The effect of a dual layer coating composed of a layer of a Co_3O_4 and a layer of a $La_{0.85}Sr_{0.15}MnO_3/Co_3O_4$ mixture on the high temperature corrosion of the Crofer 22 APU alloy is reported. Oxidation experiments were performed in dry oxygen at three temperatures: 800 °C, 850 °C and 900 °C for periods up to 1000 h. Additionally at 850 °C a 5000 h long oxidation test was performed to evaluate longer term suitability of the proposed coating. Corrosion kinetics were evaluated by measuring mass gain during oxidation. The corrosion kinetics for the coated samples are analyzed in terms of a parabolic rate law. Microstructural features were investigated by scanning electron microscopy, energy dispersive X-ray analysis and X-ray diffractometry. The coating is effective in reducing the corrosion rate and in ensuring long lifetime of coated alloys. The calculated activation energy for the corrosion process is around 1.8 eV. A complex Co–Mn–Cr spinel is formed caused by diffusion of Cr and Mn from the alloy into the Co_3O_4 coating and by additional diffusion of Mn from the LSM layer. Adding a layer of LSM/Co_3O_4, acting as an additional Mn source, on top of the cobalt spinel is beneficial for the improved corrosion resistance.

1. Introduction

Solid oxide electrolysis cells (SOECs) are very efficient devices for production of hydrogen and oxygen from steam [1]. During recent years this technology has gained a considerable attention as a promising way to store energy from time-varying resources (solar or wind power). Applying knowledge from many years of research in the field of the Solid Oxide Fuel Cells, leads to accelerated development of SOECs [2]. Beside development of the fuel electrode, the electrolyte and the oxygen electrode, interconnects must be studied and also developed to suitably fit into an SOE stack. As the working temperature of SOFCs has been lowered from about 1000 °C to 800 °C and below, the use of stainless steels for interconnects has become possible [3–5]. Many efforts have been directed to the improvement of SOFC interconnects, by development of either new alloys or coating materials [6–10]. So far studies of interconnects and its coatings for a specific use in electrolysis cells have not been carried out extensively [11–13]. The operating conditions of the electrolyzer determine the relevant corrosion atmospheres to be studied. On the fuel side it is usually a mixture of hydrogen and steam in the case of steam electrolysis (or a mixture of carbon dioxide, steam, carbon monoxide, and hydrogen in the case of co-electrolysis of steam and CO_2) and on the oxygen side it is pure oxygen that was reduced from steam on the hydrogen side and then transferred through the oxide ion conducting solid electrolyte and oxidized to oxygen molecules on the oxygen electrode. Whereas corrosion properties of interconnects and coatings are well recognized for SOFC working conditions, less is known about their behavior in SOEC specific conditions. Different atmospheres, especially with different pH_2O or pO_2 (i.e. hydrogen with different high steam content, or dry oxygen versus air), can lead to a different corrosion behavior.

Recently the need for an improved properties of interconnect in an SOE stack was highlighted by Zhang et al. [14]. One of the

* Corresponding author. Tel.: +45 46775296.
E-mail address: sebmo@dtu.dk (S. Molin).

0378-7753/$ – see front matter © 2013 Elsevier B.V. All rights reserved.
http://dx.doi.org/10.1016/j.jpowsour.2013.09.100

claimed reasons for long time stable performance of the studied SOE stack was the use of coating on the interconnect. The authors only say that the coating was based on rare-earths. As the starting point of development of coatings for SOEC stacks is based on SOFC stacks, usually similar materials and methods are used.

Recently an efficient dual layer coating was developed in our group [13,15,16]. The coating is composed of the first layer made from Co_3O_4 and a second layer being a mixture 9:1 (weight ratio) of $La_{0.85}Sr_{0.15}MnO_3$ (LSM) and Co_3O_4. Co_3O_4 was previously evaluated as a potential protective coating for interconnects [17–20]. Cobalt spinel is a very promising material to block chromium outward diffusion from the interconnect [21,22] that can lead to poisoning of the oxygen electrode [23]. LSM has also been considered as an interconnect protective material [24,25]. Both these materials have a good match with respect to thermal expansion coefficient and compatibility with cell materials. LSM is often used as an oxygen electrode, contacting paste or current collector layer on the oxygen side of the cells. The electrical conductivity of these two materials is high, being 7 S cm^{-1} for cobalt spinel [26] and >100 S cm^{-1} for LSM.

In the initial studies, the dual layer coating was tested on four different alloys (Crofer 22 APU, Crofer 22 H, E-Brite and AL29-4C) in air with 1% steam and oxygen at 850 °C for 1000 h. In comparison to the uncoated steels, dual layer coatings were effective towards reduction of the parabolic rate constants both in air with 1% steam and in oxygen [13]. It was stated that although the corrosion rates are reduced, no change in the reaction mechanism occurs.

In the present study, the dual layer coating on the Crofer 22 APU alloy is tested in dry oxygen to simulate the conditions on the oxygen side electrode of an SOE stack. In order to obtain new insight into the possible reaction mechanism and to elucidate how the lifetime is affected by temperature of operation, experiments were run at three different temperatures: 800 °C, 850 °C and 900 °C for periods up to 1000 h. Additionally, at 850 °C a 5000 h long oxidation test was performed to evaluate long term performance of the coating.

2. Experimental

The coatings were studied when applied on a 200 μm thick Crofer 22 APU (ThyssesnKrupp VDM, Germany) alloy. A steel sheet was cut into 20 × 20 mm^2 pieces and a small, 2 mm in diameter hole was punched in the coupons in order to be able to hang samples in an alumina holder. Before coating the steel coupons they were ground with a SiC paper up to #1200 grade. After polishing the samples were thoroughly cleaned in an ultrasonic bath in ethanol. The samples were then coated on both sides by a hand-held spray gun. Slurries were prepared by dispersing powders in ethanol with a small amount of binder to improve the adherence of the green coating. The first slurry was composed of only Co_3O_4 fine powder, whereas the second slurry was composed of a 9:1 (weight ratio) mixture of relatively coarse LSM and fine Co_3O_4 powders. After the deposition samples were heat treated at 850 °C for 3 h in air.

For the oxidation experiments coated samples were mounted inside an alumina sample holder and were annealed in a tube furnace at 800 °C, 850 °C or 900 °C. Heating and cooling rates were 120 °C h^{-1}. Samples were removed cyclically from the furnace after 125, 250, 500 and 1000 h and were weighed on a balance (0.01 mg resolution, Mettler Toledo). The 5000 h test samples were also weighed after 1300, 1980, 3480 and 4980 h. The average mass gain was calculated from at least 4 identical samples to ensure reproducibility. The oxidation atmosphere was pure oxygen (H_2O content ~10 ppm) flowing at 6 L h^{-1} which corresponds to a linear gas velocity of 4.5 cm min^{-1} in the alumina tube.

After oxidation experiments sample surfaces and cross sections were analyzed by scanning electron microscopy/energy dispersive X-ray analysis (SEM/EDS) using either a Zeiss Supra 35 with Noran energy dispersive X-ray spectrometer or a Hitachi TM3000 with Bruker Quantax 70 EDS system. In order to visualize cross sections, samples were cut in half by a diamond saw and embedded in epoxy and polished using 6, 3, and 1 μm diamond paste. X-ray diffraction patterns on sample surfaces were collected using a Bruker D8 Advance spectrometer with CuKα radiation at room temperature.

3. Results and discussion

3.1. Coating of samples

A cross section and a surface view of the as-prepared coating after 3 h heat treatment at 850 °C are shown in Fig. 1. The first layer made from fine Co_3O_4 powder is approximately 5–10 μm thick and the second composite layer Co_3O_4/LSM is 20–30 μm thick. The total thickness is therefore approximately 30 μm. The entire surface of the alloy is coated with this dual layer coating. Differences in thickness are due to the nature of the slurry spraying process where the thickness and uniformity of the layer cannot be controlled with a high accuracy. Thicknesses obtained in this study are on the lower limit of possible thicknesses to be produced by the slurry spraying method with uniform microstructure and even thickness over the entire sprayed area. Trying to fabricate thinner coatings could result in some areas not covered and exposed directly to the oxidizing atmosphere. Coatings prepared by slurry spraying are characterized by low green density, which is especially apparent for the LSM layer prepared from the coarse powder. On the other hand this technology is simple and the up-scaling to very large interconnects is a straightforward commercially viable process. As shown in Fig. 1, on the interface between cobalt spinel and steel already a dense reaction layer is visible which formed during the initial heat

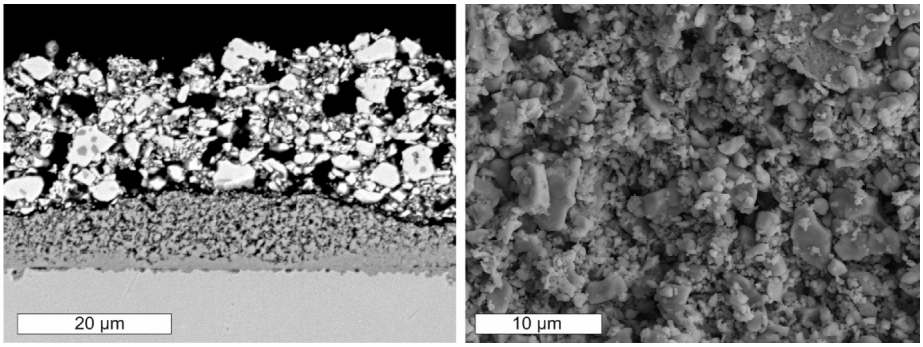

Fig. 1. SEM micrographs of cross section and surface of the dual layer coated Crofer 22 APU.

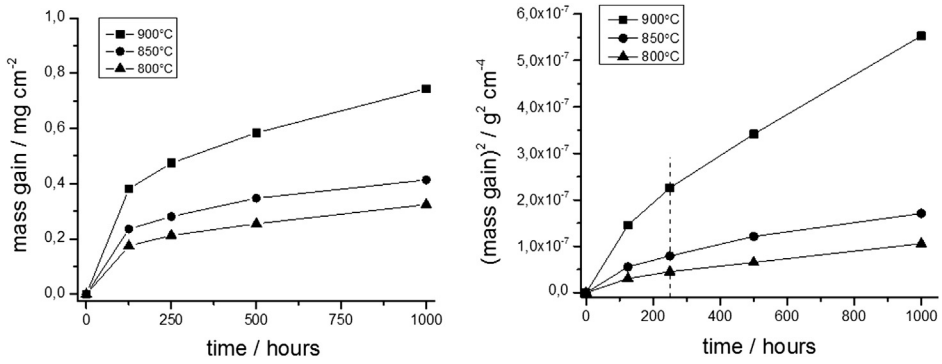

Fig. 2. Mass gain in linear and parabolic units of dual layer coated Crofer 22 APU alloys at 900 °C/850 °C/800 °C.

treatment. On the surface of the coating some large crystallites are visible, which are the coarse LSM particles. As the heat treatment temperature of 850 °C was too low to sinter the LSM and the Co_3O_4 coating, both layers are still porous.

3.2. Evaluation of corrosion kinetics

Mass gains over time of the dual layer coated Crofer 22 APU alloys measured at the three temperatures are shown in Fig. 2. Mass gains after oxidation for 1000 h at 900 °C, 850 °C and 800 °C are 0.74 mg cm^{-2}, 0.41 mg cm^{-2} and 0.33 mg cm^{-2} respectively. As expected for a thermally activated process, the higher the temperature the higher the mass gain corresponding to the formation of more corrosion products.

To determine kinetic parameters of the oxidation process usually the mass of the samples is assumed to increase with a parabolic type relationship [27]:

$$\left(\frac{\Delta m}{A}\right)^2 = k_p t + C \quad (1)$$

where Δm is a mass gain [g], A – sample area [cm^2], k_p – corrosion rate [$g^2\ cm^{-4}\ s^{-1}$], t – oxidation time [s], C – integration constant [$g^2\ cm^{-4}$].

A parabolic type expression will describe the corrosion process if the rate is limited by a diffusion process either by cation or anion diffusion. It is generally accepted that for high temperature corrosion processes occurring in SOFC/SOEC relevant conditions a limiting factor is chromium outward diffusion from the alloy. The integration constant C can be assigned to initial transient phenomena during oxide growth.

Mass gains of the samples are plotted in parabolic units in Fig. 2. To analyze the data two approaches were considered. In the first one, Equation (1) with the integration constant C was used for fitting (between 150 and 1000 h) and in the second case, the obtained curve was fitted by two parabolic type expressions, one used between 0 and 250 h and second between 250 and 1000 h. By this treatment we are assuming that different processes take place during the initial phase and at the later stage due to the complex nature of the dual layer coating and its interaction with Cr and Mn from the alloy.

Calculated corrosion rates and constants C from the two approaches are given in Table 1. Comparing obtained k_p values, the highest corrosion rates are found during the initial oxidation period (0–250 h). The values (k_{p1}) are approximately two times higher than the corrosion rates determined for the later stage (k_{p2}, 250–1000 h). On the other hand, corrosion rates obtained from a single line fitting between 150 and 1000 h (k_p) are only slightly higher than the k_{p2} value from dual line fitting. Initial higher oxidation rates can be attributed to several possible phenomena. For an uncoated Crofer 22 APU steel, during the initial period of the oxidation Cr and Mn diffuse out of the alloy to form a layered oxide scale on the surface. The first layer is always composed of Cr_2O_3 and second, outer layer of a $(Mn,Cr)_3O_4$ spinel. In case of a dual layer coating, Co can form a solid solution with Mn and Cr as well. The inner part of the coating is a reaction zone where cations from the steel can diffuse to and form a thermodynamically stable oxide in combination with the coating layer. A broad composition range exists for the spinel phase in the Mn–Co–Cr–O system [15] and therefore it is not possible at this stage to give a specific composition of the spinel. In order for Cr to diffuse to the outer coating, cations have to diffuse through three layers (Cr_2O_3, (MnCr) spinel, and Co spinel). In the case of a single line fitting, the integration constant C has no easily attributable physical meaning. It is evident that the value of C is decreasing with the decrease of temperature. It is expected that this is simply a different manifestation of the processes described by a dual line fitting.

At this stage it is difficult to conclude which of the two analysis approaches is better. None of them precisely describes the oxidation rate. For lifetime prediction, the k_{p2} corrosion rate obtained from the dual-line fitting should be more relevant to use, as the initial corrosion process is rather short as compared to the expected IC service time (>40,000 h). Using k_p values from single-line fitting would underestimate the predicted lifetime.

In general, data for oxidation of Crofer 22 APU in pure oxygen are scarce so also results from oxidation experiments carried out in air will be included for an indirect comparison. As presented by Palcut et al. the corrosion rate of Crofer 22 APU in oxygen at 850 °C

Table 1
Calculated k_p and C values for oxidation of dual layer coated samples.

Temperature	Single line fitting[a]		Dual line fitting[a]	
	k_p [$\times 10^{-14}\ g^2\ cm^{-4}\ s^{-1}$]	C [$\times 10^{-7}\ g^2\ cm^{-4}$]	k_{p1} [$\times 10^{-14}\ g^2\ cm^{-4}\ s^{-1}$]	k_{p2} [$\times 10^{-14}\ g^2\ cm^{-4}\ s^{-1}$]
900 °C	12.70	1.022	25.0	12.07
850 °C	3.59	0.461	8.78	3.30
800 °C	2.33	0.222	5.03	2.23

[a] Value k_p corresponds to fitting between 150 and 1000 h, k_{p1} to 0–150 h and k_{p2} to 250–1000 h.

is 10 times higher than in air at the same temperature [12]. For a similar dual layer coating on Crofer 22 APU tested in air at 850 °C the obtained k_p value was 7.39×10^{-14} g^2 cm^{-4} s^{-1} about two times higher than the one obtained in this study. The difference might be caused by a different moisture content, surface preparation and different slurry composition (different powders used for the preparation of the slurry). In another study, a plasma sprayed LSM protective coating was deposited on Crofer 22 APU and oxidized in oxygen at 850 °C. The coated samples had a k_p value of 19.0×10^{-14} g^2 cm^{-4} s^{-1}, 5–6 times higher than found here for the dual layer coatings.

For oxidation in air, Crofer 22 APU have k_p values of 6.49×10^{-14} g^2 cm^{-4} s^{-1} and 1.00×10^{-12} g^2 cm^{-4} s^{-1} at 800 °C and 900 °C respectively [28]. These values are also much higher than for the coated samples oxidized in oxygen reported here. From the above comparison it is evident that the dual layer coating is effective in reducing corrosion rates. In comparison of the data it must however be taken into account that the obtained k_p values can also be dependent on the moisture content [29–31].

The beneficial effect of adding a second layer can be discussed by comparing to the results obtained by Persson et al. [15,16]. In this study a 7 μm and 15 μm thick Co_3O_4 porous coating deposited on Crofer 22 APU resulted in a decreased corrosion rate in air (with 1% of steam) at 900 °C. The corrosion rate was decreased to approximately half (from 8.2×10^{-13} g^2 cm^{-4} s^{-1} to $\sim 4 \times 10^{-13}$ g^2 cm^{-4} s^{-1}). After adding a second layer of LSM on top of the cobalt spinel, further decrease of the corrosion rate was achieved (to a value of 5.4×10^{-14} g^2 cm^{-4} s^{-1}). The LSM acts possibly as a source of elements for improved scale adherence (La) and surely as an Mn source. It was recently shown that a 200 μm thick Fe22Cr alloy oxidized for 3000 h at 850 °C was completely depleted in Mn, so adding an external source of this element can possibly bring some long term benefits [32].

The temperature dependences of the k_p parameters from the dual line fitting are plotted in Fig. 3. Slopes are similar between the two periods. The corresponding activation energies can be calculated by fitting the data by an Arrhenius type equation:

$$k_p(T) = k_{p0}\exp\left(-\frac{E_A}{k_B T}\right) \quad (2)$$

where $k_p(T)$ – corrosion rate [g^2 cm^{-4} s^{-1}], k_{p0} – corrosion rate constant [g^2 cm^{-4} s^{-1}], E_A – activation energy [eV], k_B – Boltzmann constant [eV K^{-1}], T – temperature [K].

Activation energies obtained for 0–250 h and 250–1000 h are 1.73 eV and 1.81 eV respectively. It seems that reaction rates for the initial process are approximately 2 times faster than for the later stage but the activation energy remains similar which might imply that the rate-limiting step is the same in both cases. One of the expected limiting factors for formation of the oxide scale is the outward diffusion of Cr and Mn from steel.

For the uncoated Crofer 22 APU oxidized in dry O_2 at 850 °C an activation energy of 2.61 eV was reported by Palcut et al. [12]. In this case the process responsible for the corrosion rate was described as the limiting outward diffusion in the Cr_2O_3 oxide scale. In the case of dual layer coated samples, the activation energy is considerably smaller, probably due to much more complicated diffusion fluxes and the fact that the composition of the scale changes over time. Douglass et al. [33] have reported an activation energy of 2.15 eV for the formation of a Co–Cr–Mn spinel on a Co–20Cr alloy.

3.3. Microstructural characterization

After collection of mass gain data, the samples were characterized by XRD to analyze the phase composition of the coating and the oxide scale. X-ray diffractograms of oxidized dual layer coated Crofer 22 APU are presented in Fig. 4. For the as-coated sample without any heat treatment peaks originating from LSM (ICDD File card no. 49-595) and Co_3O_4 (ICDD File card no. 43-1003) are detected. Due to the total thickness of the coating being >30 μm no peaks from the steel substrate are visible and low intensity of Co_3O_4 peaks means that mainly the outer LSM based layer is analyzed by the X-ray beam. Already after initial 3 h heat treatment in air at 850 °C the obtained diffractogram looks different. Peaks from the cobalt spinel are not visible anymore. Also for oxidized samples (either 1000 or 5000 h) no cobalt spinel peaks are detected. Small amount of Co_3O_4 in the outer layer might have reacted with LSM or products diffusing from the steel. It is evidenced by formation of a spinel type product, which can be assigned well to a $(Mn,Cr,Co)_3O_4$ cubic spinel (ICDD File card no. 70-2465). Mn from LSM reacts with Co and forms a spinel phase that further reacts with Cr forming a more complex spinel. A shift of the LSM peaks towards higher 2θ angles is observed, which corresponds to a decrease in the unit cell size of the LSM. The longer the oxidation time the stronger the shift. One possible explanation can be that Co from the spinel that was part of the outer layer is incorporated into the LSM structure. The ionic size of the Co^{+3} is smaller (0.545 nm) than the size of the Mn^{3+} (0.58 nm) so a decrease of the unit cell size is expected. This is confirmed by the XRD, where the Co_3O_4 phase is not longer detected after the oxidation. From the XRD measurement it is also

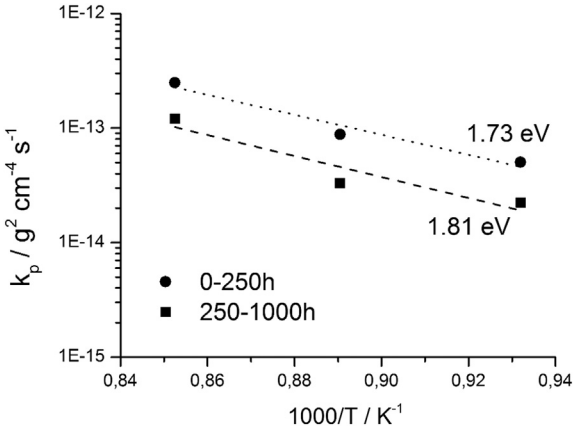

Fig. 3. Temperature dependance of corrosion rates.

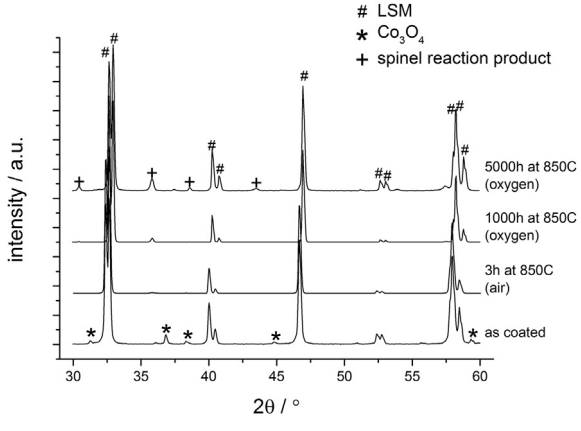

Fig. 4. XRD diffractograms of dual layer coated alloys oxidized for different times at 850 °C.

observed that the intensity of the Mn,Cr,Co spinel phase peaks becomes higher with longer oxidation times.

To further analyze the surface of the dual layer coated samples energy dispersive X-ray spectrometry was performed on sample oxidized for 1000 h at 850 °C. An SEM image of the sample surface and chemical composition of the points from EDS point analysis are presented in Fig. 5.

In Fig. 5 one large crystallite is visible. Chemical analysis performed at two points (Point 1 and Point 2) reveals that the most abundant element in the particle is chromium. Additionally it is rich in cobalt, manganese and has smaller amounts of lanthanum and strontium. Such a chromium rich particle on the surface of sample oxidized for 1000 h in oxygen suggests a considerable diffusion of chromium through the dual layer coating. As the total coating thickness is on average 30 μm the Cr diffusion rate is considerable. The rectangular particle (including points 1 and 2) is most likely a spinel phase. In Point 3 there is the least amount of chromium among the analyzed points. It reaches 0.37 at.%. This point is rich in La, Mn and can be assigned to the LSM perovskite. Points 4, 5 and 6 are also based on La and Mn, with Cr content between 4 and 6 at.%. As the main conclusion from this analysis, it must be stated that a considerable amount of Cr is found on the surface of a dual layer coated samples. As the setup used for oxidation was based on an alumina tube and there were no bare steel elements subjected to oxidation inside the hot zone, the chromium has diffused through the coating either by a solid state diffusion probably on the surface of the particles in the coating or via a vapor deposition process [34]. In the dry oxygen atmosphere with low steam content, transport of chromium through a gas phase is probably insignificant [35].

The cross-sections of the samples were also characterized using SEM&EDS. Micrographs of polished cross sections of dual layer coated samples oxidized for 1000 h at 800 °C, 850 °C and 900 °C are shown in Fig. 6. Additionally elemental maps of Cr, Co and Mn are included. Due to the reactive nature of the dual layer coating, corrosion products are not clearly distinguishable. Next to the steel a Cr_2O_3 layer is visible as a dark layer. Next is a Mn,Co,Cr spinel that forms by reaction of the Co_3O_4 coating with Mn and Cr diffused from the steel. For bare Crofer 22 APU on top of the chromia scale a Mn,Cr spinel is normally formed. As evidenced by the surface EDS analysis, the diffusion of Cr occurs through entire thickness of the coating. Presence of Cr in the coating is also visible on the Cr elemental maps. From the comparison of the elemental maps in the outermost layer it can be seen that the Cr is present in the same places as the Co. Comparing Mn elemental maps after oxidation at three temperatures, it can be seen that in the case of the lowest oxidation temperature (800 °C), the Mn is present more at both interfaces of the Co_3O_4 layer than in the middle of this layer. For higher temperatures (850 and 900 °C) the distribution of Mn is more homogenous. It evidences the fact that the Mn diffuses both from the steel and from the coating into the reaction zone. The thickness of the Cr_2O_3 layer after 1000 h of oxidation at 800 °C is ~2 μm.

Fig. 7 shows a cross section of a sample oxidized at 800 °C for 1000 h together with EDS point analysis. Point 1 is rich in La, Sr, Mn and Co and is the second layer of the coating. Moreover on average 2.2 at.% chromium is detected which is in agreement with previously described chromium diffusion. Point 2, lying at the interface between LSM/Co_3O_4 and Co_3O_4, is rich in Co and Mn. Mn probably comes from the outer LSM rich layer. This interface is forming a thin dense layer. Inside the porous reaction zone, Point 3 is rich in cobalt with smaller additions of Mn and Cr at a level of approximately 5 at.%. Below this layer a dense reaction layer exists with the composition rich in cobalt and with increased amounts of Mn and Cr reaching 10% (Point 2). Within the composition ranges found in Points 2, 3 and 4 Co–Mn–Cr form a single phase cubic spinel [15]. Next to the steel, Point 5 is rich in chromium. Also some amount of Mn and negligible Co are detected. This layer is primarily a chromium oxide phase. It is interesting to note, that the both dense Co,Cr,Mn layers, located on the both sides of the Co_3O_4 coating, were more rich in Cr and Mn than in the case of the porous spinel found in the middle.

Relatively high concentration of chromium found throughout the coating means that the porous Co_3O_4 layer is not protective against diffusion of Cr. Among the materials for potential use for interconnect coatings, the Co_3O_4 spinel in a dense form is the most effective material to block chromium diffusion [22]. Evaporation of Cr from the surface of the steel or the surface of the coating to the active cathode can lead to poisoning of the cathode reaction in the fuel cell (anode in the electrolysis cell) [22,32]. Another material, reported to be effective in reducing Cr poisoning, is a Mn,Co spinel (e.g. $MnCo_2O_4$ or $Mn_{1.5}Co_{1.5}O_4$) [7,36,37]. The possible influence of Cr poisoning of the SOEC oxygen electrode has still not been reported in detail in literature. Due to different polarization of the oxygen electrode in the SOEC mode and a very low moisture content of the generated oxygen, Cr poisoning in SOEC stacks should be less severe than in SOFC stacks. In the case of deposited porous cobalt spinel, Co reacts with Cr and Mn and readily forms a Cr rich phase. In the case of Mn,Cr spinels, it was shown that chromium ions diffuse through high diffusivity paths, e.g. grain boundaries [38]. The porous coating will be susceptible to chromium diffusion and cannot effectively block chromium migration. It is still expected however that the chromium evaporation is strongly reduced by the dual layer coating as the chromium activity is significantly lowered.

Mixed spinels of Mn–Co–Cr are reported to have a thermal expansion coefficient close (~12 ppm K^{-1}) to that of the materials used in SOEC construction. Also electrical conductivity of these spinels is usually considerably higher than that of chromia (for pure Mn,Co spinels up to 60 S cm^{-1} at 800 °C whereas for chromia it is in the range of few mS cm^{-1}) [39].

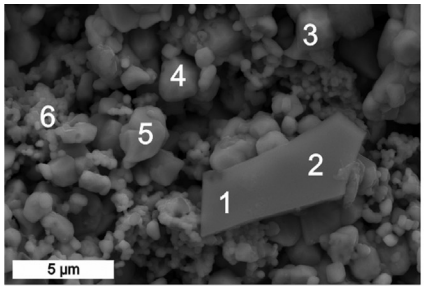

(at.%)	Point 1	Point 2	Point 3	Point 4	Point 5	Point 6
La	4.13	3.09	20.92	17.88	16.57	12.49
Sr	0.50	0.40	3.62	2.23	2.27	1.99
Mn	8.23	7.40	20.69	14.48	14.51	13.33
Co	10.53	10.44	2.87	3.18	3.02	5.72
Cr	15.38	15.81	0.37	5.96	3.75	5.13
O	61.23	62.86	51.52	56.27	59.78	61.34

Fig. 5. SEM image of the surface after 1000 h of oxidation at 850 °C together with EDS point analysis (at.%).

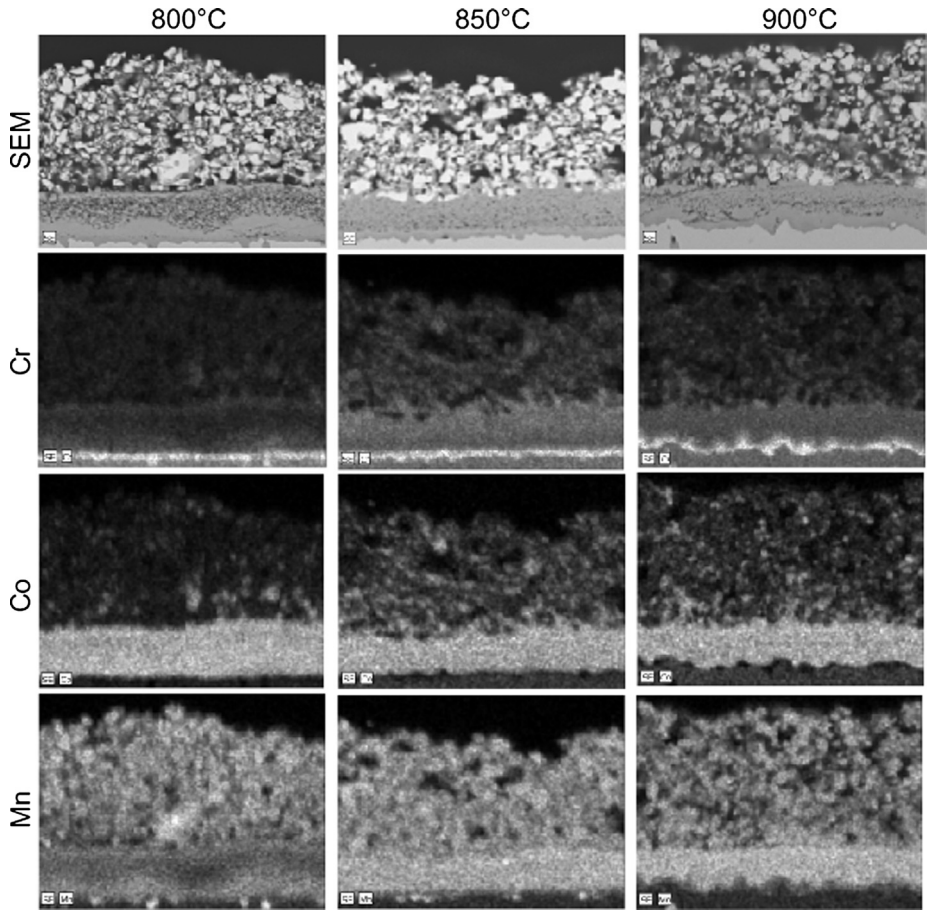

Fig. 6. SEM images and EDS elemental maps (Cr, Co and Mn) of samples oxidized at different temperatures for 1000 h.

3.4. Extended oxidation time at 850 °C

Many reported corrosion studies of SOFC/SOEC interconnects are performed over relatively short times ~1000 h, from which materials behavior is then extrapolated on the base of the parabolic rate law. This method is assuming that no changes in the corrosion mechanism will occur with prolonged oxidation time. However, as the chromium level in the alloy can fall below the protective limit (~16 wt.%), a drastic change in the corrosion rate can be observed [28]. A limited number of studies exist, where corrosion properties have been reported for periods considerably longer than 1000 h [16,40,41].

The long term (5000 h) mass gain of a dual layer coated Crofer 22 APU is presented in Fig. 8a. A small departure from parabolic type behavior is seen. The mass gain in "parabolic units" is shown in Fig. 8b. Here the fitting of the k_p value is performed between 150 and 5000 h. The calculated k_p is equal to 2.76×10^{-14} g^2 cm^{-4} s^{-1} and constant C is equal $C = 0.86 \times 10^{-7}$ g^2 cm^{-4}. Comparing with the values obtained for 1000 h oxidation, the value from the 5000 h study is lower by approximately 25%. The obtained k_p value can be used to calculate oxide thickness after 5 years (~44,000 h) of the operation of the SOEC stacks. Main concern in this case is the increase of the electrical resistivity due to increase in thickness of the poorly conductive oxide layer (in terms of the Area Specific Resistance) and spalling-off of the oxide scale due to a mismatch of the thermal expansion coefficient (TEC). The TEC of the Crofer 22 APU alloy is 12.4 ppm K^{-1} whereas TEC of the Cr_2O_3 is 9.6 ppm K^{-1} [42]. Usually a practical limit of 10 μm thick oxide scale is used as an indicative number for when risk of spallation becomes significant and resistivity becomes high. Electrical conductivity of the chromia

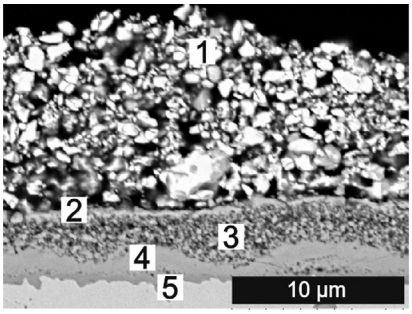

(at.%)	Point 1	Point 2	Point 3	Point 4	Point 5
La	16.5	0	0	0	0
Sr	3.2	0	0	0	0
Mn	22.0	7.8	4.8	8.2	10.1
Co	6.9	32.8	42.5	30.0	1.5
Cr	2.2	7.7	5.8	10.4	35.2
O	49.1	51.4	46.6	51.2	52.9

Fig. 7. SEM image of the cross section after 1000 h of oxidation at 800 °C together with EDS point analysis (at.%).

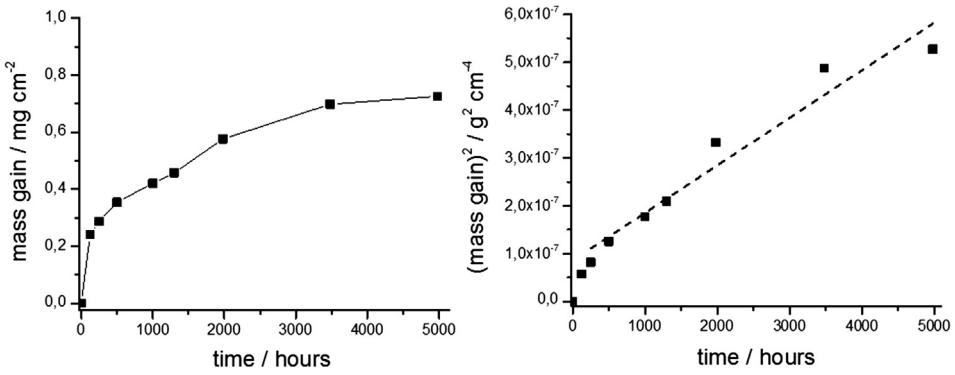

Fig. 8. Mass gain in linear and parabolic units of dual layer coated Crofer 22 APU alloys at 850 °C oxidized for 5000 h.

scale is in the order of 0.006–0.16 S cm^{-1} [39,42–44]. Assuming formation of a 10 μm thick chromia scale, ASR of between 0.16 and 0.006 Ω cm^2 can be calculated. Oxide scale thickness after 5 years of operation calculated from the given k_p value is around 4 μm in case of a dual layer coating in pure oxygen at 850 °C. The limiting thickness of 10 μm will be reached after 250,000 h (28 years) of operation. From this rough extrapolation long term (exceeding 5 years) operation with the dual layer coating seems feasible even in this highly oxidizing atmosphere. Using k_p values from Table 1, time to reach a 10 μm thick scale at 900 °C and 800 °C can be estimated. In these cases, the thickness of 10 μm will be reached after 55,000 h (~6 years) and 300,000 years (34 years) respectively.

These lifetime predictions are based on the limiting oxide scale thickness that contribute to the resistance of the interconnect. Clearly, the dual-layer coating results in reduced Cr oxide scale thickness, which is poorly conductive and therefore the electrical conductivity of coated alloy should be superior in comparison to that of the not coated one. However due to a complicated nature and composition of formed oxides these calculations should be taken only as qualitative indications. Performing dedicated area specific resistance measurements would be required to fully describe the properties of this coating, which is beyond the scope of this publication and will be presented elsewhere.

The difference between the k_p values obtained from the initial 1000 h and a 5000 h shows that the corrosion process does not follow exactly the parabolic rate law over the whole studied time. In the case of the reactive coating, not only the thickness increase occurs but also simultaneously due to composition changes of the reactive layer the transport properties are affected, i.e. the effective Cr diffusion coefficient changes over time. Potentially also the effect of a limited Cr reservoir in the alloy (in this case the alloy was only 200 μm thick) can over long time cause deviation from a pure parabolic rate equation, which assumes a constant and an infinite source of the available Cr. Also, due to a reactive nature of the porous coating, a given mass gain ascribable to Cr or Mn oxidizing effectively adds more thickness (corrosion reaction extends further) due to the reaction with the particles in the porous layer. In general, by a complex reaction of the diffusing species with the reactive coating some additional protection mechanism is added (the apparent k_p decreases over time).

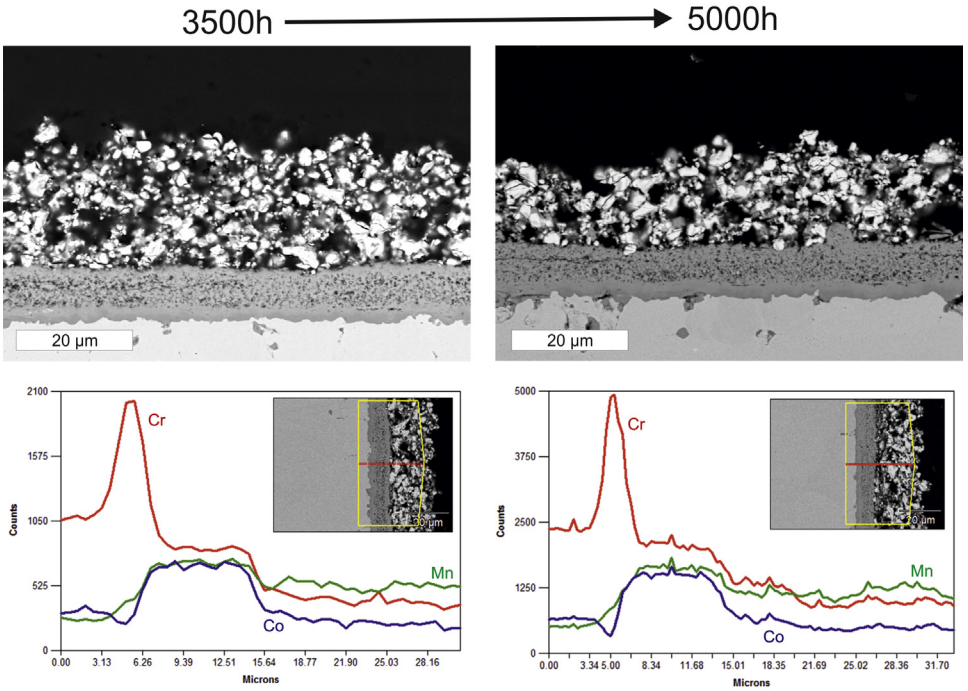

Fig. 9. Cross sections of dual layer coated alloys oxidized for 3500 and 5000 h at 850 °C with elemental line scans.

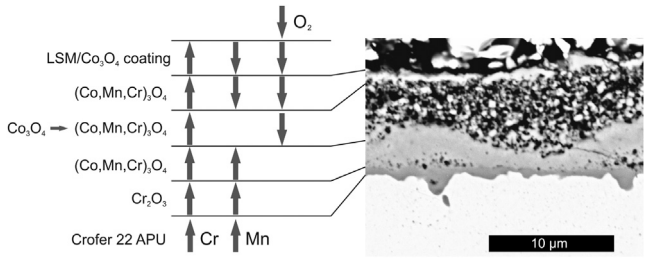

Fig. 10. Schematic of diffusion fluxes and formation of reaction layers in a dual layer coated sample.

Polished cross section images of coated samples after 3500 and 5000 h of oxidation are shown in Fig. 9a together with elemental line scans in Fig. 9b. As previously reported, the first layer is a chromia scale on top of which a reaction layer exists. The reaction zone is dense just next to the chromia scale. On top of the coating is still a porous layer, followed again by a denser structure on the interface between LSM and the Co based spinel. Comparing images taken after 1000 h, 3500 h and 5000 h no very evident differences in thickness of the chromia scale are detected. Interdiffusion of Co, Cr and Mn is evident from the elemental line scans. The level of Mn throughout the reaction zone is constant. Mn diffuses from the steel and from the LSM coating leading to an equal distribution of the Mn throughout the reaction layer.

In Fig. 10 a schematic of the possible element fluxes is included next to the cross section of the sample after 1000 h of oxidation in oxygen at 800 °C. Chromium diffuses from the alloy through all layers, forming a Cr_2O_3 layer and then a mixed spinel with a Co_3O_4 coating. Mn from the alloy diffuse trough the chromia scale (very low solubility of Mn in Cr_2O_3) to the cobalt spinel phase and reacts with it. An additional flux of Mn comes from the LSM coating above the Co_3O_4. Mn enriched layers are formed on both interfaces of the porous Co_3O_4 coating. Due to the porous nature of coatings, oxygen from the oxidizing gas is expected to diffuse via the gas phase.

4. Conclusions

In the present study, the effect of a dual layer coating on the corrosion resistance of a Crofer 22 APU alloy has been evaluated. The developed dual layer coating is effective in lowering corrosion rates. The corrosion rate constant at 850 °C is lowered from 189×10^{-14} g^2 cm^{-4} s^{-1} [12] for the uncoated alloy to around 3.6×10^{-14} g^2 cm^{-4} s^{-1} for the dual layer coated Crofer 22 APU. Without the coating it would not be possible to use this alloy for more than approximately 1000 h (assuming end of life at 10 μm scale thickness). The coating extends the lifetime of the alloy considerably. From the temperature dependence of the corrosion rates an activation energy of the oxidation process was calculated to be approximately 1.8 eV. This is lower than reported for non coated Crofer 22 APU. This is due to a complex interaction between the coating and the diffusing elements (Cr and Mn ions). Next to the steel, the oxide scale consists of first a chromia layer, a dense reaction layer, a porous reaction layer, and again a denser thin layer which is formed by interdiffusion of Mn from the LSM coating into the cobalt spinel coating. All these reaction layers are composed of Co–Cr–Mn, where the dense interlayers are richer in Mn and Cr than the porous layer. Relatively large amount of Cr is found throughout the coating and on the surface (up to 16 at.%). On average few percent of chromium is found close to the surface of the 30 μm thick coating after 1000 h oxidation, indicating significant outward Cr diffusion. In general it is concluded that Crofer 22 APU coated with the dual layer coating is a promising interconnect material for Solid Oxide Electrolysis Stacks for operation even at elevated temperatures and in oxidizing atmospheres.

Acknowledgments

Financial support from Energienet.dk through the ForskEL project number 2011-1-10609 “Development of SOEC cells and stacks” is gratefully acknowledged. Pernille Hedemark Nilesen is acknowledged for metallographic sample preparation.

References

[1] M.A. Laguna-Bercero, J. Power Sources 203 (2012) 4–16.
[2] P. Hjalmarsson, X. Sun, Y.-L. Liu, M. Chen, J. Power Sources 223 (2013) 349–357.
[3] S. Linderoth, J. Electroceram. 22 (2009) 61–66.
[4] S. Linderoth, P.V. Hendriksen, M. Mogensen, N. Langvad, J. Mater. Sci. 31 (1996) 5077–5082.
[5] G. Cabouro, G. Caboche, S. Chevalier, P. Piccardo, J. Power Sources 156 (2006) 39–44.
[6] N. Shaigan, W. Qu, D.G. Ivey, W. Chen, J. Power Sources 195 (2010) 1529–1542.
[7] Y. Larring, T. Norby, J. Electrochem. Soc. 147 (2000) 3251–3256.
[8] X. Montero, N. Jordan, J. Piron-Abellan, F. Tietz, D. Stover, M. Cassir, I. Villarreal, J. Electrochem. Soc. 156 (2009) B188–B196.
[9] J.W. Fergus, Mater. Sci. Eng. A 397 (2005) 271–283.
[10] J.W. Fergus, Scr. Mater. 65 (2011) 73–77.
[11] J. Yoo, S.-K. Woo, J.H. Yu, S. Lee, G.W. Park, Int. J. Hydrogen Energy 34 (2009) 1542–1547.
[12] M. Palcut, L. Mikkelsen, K. Neufeld, M. Chen, R. Knibbe, P.V. Hendriksen, Corros. Sci. 52 (2010) 3309–3320.
[13] M. Palcut, L. Mikkelsen, K. Neufeld, M. Chen, R. Knibbe, P.V. Hendriksen, Int. J. Hydrogen Energy 37 (2012) 14501–14510.
[14] X. Zhang, J.E. O'Brien, R.C. O'Brien, J.J. Hartvigsen, G. Tao, G.K. Housley, Int. J. Hydrogen Energy 38 (2013) 20–28.
[15] Å.H. Persson, L. Mikkelsen, P.V. Hendriksen, M.A.J. Somers, J. Alloys Compd. 521 (2012) 16–29.
[16] Å.H. Persson, High Temperature Oxidation of Slurry Coated Interconnect Alloys (Ph.D. Thesis), Department of Energy Conversion and Storage, Technical University of Denmark, 2012.
[17] M. Burriel, G. Garcia, J. Santiso, A. Hansson, S. Linderoth, A. Figueras, Thin Solid Films 473 (2005) 98–103.
[18] A.N. Hansson, S. Linderoth, M. Mogensen, M.A.J. Somers, J. Alloys Compd. 433 (2007) 193–201.
[19] A.N. Hansson, M. Burriel, G. Garcia, S. Linderoth, M.A.J. Somers, Oxid. Met. 68 (2007) 23–36.
[20] X. Deng, P. Wei, M.R. Bateni, A. Petric, J. Power Sources 160 (2006) 1225–1229.
[21] J. Froitzheim, H. Ravash, E. Larsson, L.G. Johansson, J.E. Svensson, J. Electrochem. Soc. 157 (2010) B1295–B1300.
[22] R. Trebbels, T. Markus, L. Singheiser, J. Fuel Cell Sci. Technol. 7 (2010) 011013.
[23] L.G.J. De Haart, A. Neumann, N.H. Menzler, I.C. Vinke, ECS Trans. 35 (2011) 2027–2033.
[24] M. Palcut, L. Mikkelsen, K. Neufeld, M. Chen, R. Knibbe, P.V. Hendriksen, Int. J. Hydrogen Energy 37 (2012) 8087–8094.
[25] J.-J. Choi, J. Ryu, B.-D. Hahn, W.-H. Yoon, B.-K. Lee, J.-H. Choi, D.-S. Park, J. Alloys Compd. 492 (2010) 488–495.
[26] A. Petric, H. Ling, J. Am. Ceram. Soc. 90 (2007) 1515–1520.
[27] P. Kofstad, High Temperature Corrosion, Elsevier Applied Science Publishers, London and New York, 1988.
[28] P. Huczkowski, V. Shemet, J. Piron-Abellan, L. Singheiser, W.J. Quadakkers, N. Christiansen, Mater. Corros. 55 (2004) 825–830.
[29] H. Buscail, R. Rolland, C. Issartel, F. Rabaste, F. Riffard, L. Aranda, M. Vilasi, J. Mater. Sci. 46 (2011) 5903–5915.
[30] S. Fontana, S. Chevalier, G. Caboche, J. Power Sources 193 (2009) 136–145.
[31] S.R.J. Saunders, M. Monteiro, F. Rizzo, Prog. Mater. Sci. 53 (2008) 775–837.
[32] J. Froitzheim, S. Canovic, M. Nikumaa, R. Sachitanand, L.G. Johansson, J.E. Svensson, J. Power Sources 220 (2012) 217–227.
[33] D.L. Douglass, J.S. Armijo, Oxid. Met. 3 (1971) 185–202.
[34] G.Y. Lau, M.C. Tucker, C.P. Jacobson, S.J. Visco, S.H. Gleixner, L.C. DeJonghe, J. Power Sources 195 (2010) 7540–7547.
[35] K. Hilpert, J. Electrochem. Soc. 143 (1996) 3642–3647.
[36] E. Alvarez, A. Meier, K.S. Weil, Z. Yang, Int. J. Appl. Ceram. Technol. 8 (2009) 33–41.
[37] B. Hua, J. Pu, W. Gong, J. Zhang, F. Lu, L. Jian, J. Power Sources 185 (2008) 419–422.
[38] J. Gilewicz-Wolter, J. Dudała, Z. Żurek, M. Homa, J. Lis, M. Wolter, J. Phase Equilib. Diffus. 26 (2005) 561–564.
[39] K. Wang, Y. Liu, J.W. Fergus, J. Am. Ceram. Soc. 94 (2011) 4490–4495.
[40] J. Malzbender, P. Batfalsky, R. Vaßen, V. Shemet, F. Tietz, J. Power Sources 201 (2012) 196–203.
[41] S. Fontana, S. Chevalier, G. Caboche, Mater. Corros. 62 (2011) 650–658.
[42] Z.H. Bi, J.H. Zhu, S.W. Du, Y.T. Li, Surf. Coat. Technol. 228 (2013) 124–131.
[43] J.H. Park, K. Natesan, Oxid. Met. 33 (1990) 31–54.
[44] S.C. Tsai, A.M. Huntz, C. Dolin, Oxid. Met. 43 (1995) 581–596.